ACS Photonics

Perspective

pubs.acs.org/journal/apchd5

Photonics and Plasmonics in 4D Ultrafast Electron Microscopy

Brett Barwick[†] and Ahmed H. Zewail*[,‡]

[†]Department of Physics, Trinity College, Hartford, Connecticut 06106, United States

[‡]Physical Biology Center for Ultrafast Science and Technology, Arthur Amos Noyes Laboratory of Chemical Physics, California Institute of Technology, Pasadena, California 91125, United States

ABSTRACT: Light−matter interactions at the nanoscale are fundamental to the rapidly developing fields of plasmonics and nanophotonics. These fields hold the promise of advancing both the speed of computers along with communications and may also provide methods to create a new generation of ultrasensitive molecular biosensors. While there are a variety of techniques that can provide static images of these devices with suboptical wavelength precision there are only a few that are capable of capturing the ultrafast dynamics of electromagnetic fields interacting with or produced by nanomaterials. In this Perspective, we aim to introduce the reader to the newly developed field of 4D ultrafast electron microscopy (4D UEM), which provides a unique window into ultrafast dynamics at the nanoscale. We will describe the basic technique and how internal structural, bulk electronic, and surface near-field dynamics can all be obtained with nanometer and femtosecond resolutions. In addition, we will discuss how a variety of different ultrafast electron microscopes have been used to map the evolution of photonics-related phenomena. Throughout, we discuss the direction of research that will help advance the understanding of light−matter interactions near the atomic scale in both space and time.

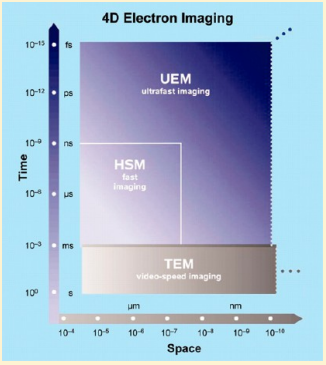

KEYWORDS: *plasmonics, nanophotonics, UEM, SUEM, UPPEM, PINEM, electronic dynamics, structural dynamics*

Recent advancements in the field of 4D UEM[1] have shown that a variety of phenomena[2,3] can be observed with femtosecond and nanometer resolutions, including the ability to follow bulk electronics in materials and near-fields of laser excited surfaces around nanoobjects. The diverse set of ultrafast electron microscopes that have been developed provide for future investigations of these phenomena, which relate to photonics and plasmonics and the ultrafast behavior of nanooptical effects.[4] Two commonly used instruments to obtain static images for the characterization of plasmonic and nanophotonic devices are the scanning electron microscope and the transmission electron microscope. Introducing the fourth dimension (time) to these microscopes so that they can capture ultrafast dynamics has the potential to unravel the mechanism of not only structural dynamics in materials, but also the dynamics of optical fields coupling with matter on the nanometer scale.

With the promise of plasmonics[5] to enhance future computers and create a better generation of molecular sensors, new techniques must be developed that image these next generation devices and are also capable of following their ultrafast dynamical behavior, on the time and spatial scales of the phenomena. At the heart of each plasmonic device is the interaction between the electrons in and on the surface of the material and the electromagnetic wave incident on it. On the nanoscale, these two cannot be decoupled and imaging each is necessary to better understand how they are coupled and evolve in ever more complicated structures. The ultimate goal for imaging plasmon dynamics in UEM is to be able to follow the bulk electronic and surface near-fields with a temporal resolution near a few femtoseconds, which is the natural time scale for electrons oscillating in a visible optical field.

■ DEFINITIONS AND MISNOMERS

Introducing temporal resolution to electron microscopy allows for fast and ultrafast imaging of nanoscale dynamics. For fast processes, which include those that can be followed using nanosecond lasers, dynamics can be obtained with nanosecond to microsecond temporal resolutions (to avoid definitional confusion that has cropped up in the literature,[6] we will refer to this regime as high speed imaging). Ultrafast has typically been defined in the laser community as picosecond and faster;[7] this definition persisted for decades, and we adopt such definition when discussing ultrafast electron microscopy. While high speed electron microscopy techniques are very useful for imaging irreversible structural and material changes,[8] they are not capable of following most electronic processes which have much faster dynamics. Single-pulse electron imaging is also relatively limited in its ability to spatially resolve structures, due to Coulomb repulsion in the imaging electron pulse and is limited to 10−100 s of nanometers resolution.[8] This is in contrast to ultrafast electron microscopy techniques employing single-electron imaging, which can reach atomic-scale resolution.[9] The boundaries between these different spatiotemporal electron imaging regimes is depicted in Figure 1.

Received: July 31, 2015
Revised: August 26, 2015
Accepted: August 27, 2015
Published: September 24, 2015

DOI: 10.1021/acsphotonics.5b00427
ACS Photonics 2015, 2, 1391−1402

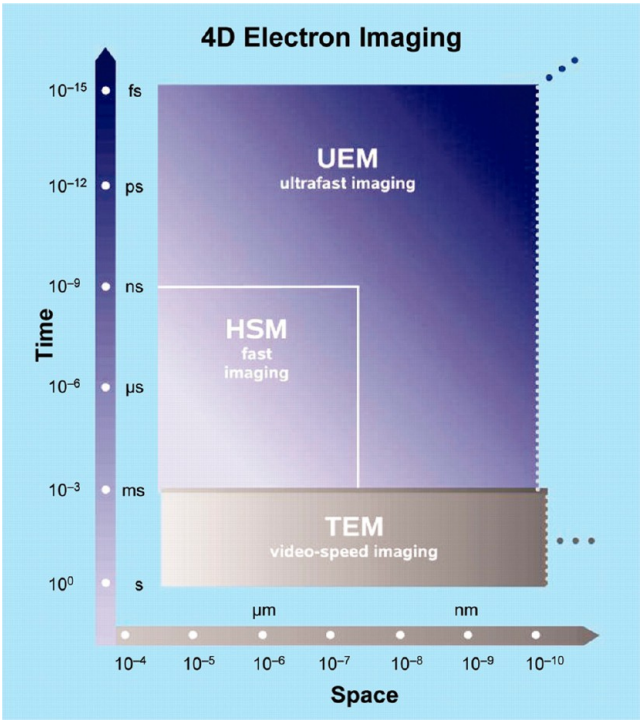

Figure 1. 4D electron imaging. The resolution boundaries of ultrafast imaging are compared with those achieved in conventional TEM, limited by the speed of video camera, and, in high-speed microscopy (HSM), defined by the rectangle shown. The spatiotemporal scales of UEM achieved to date are outlined with possible future extensions. Figure is adapted with permission from ref 1. Copyright 2010 AAAS.

4D ULTRAFAST ELECTRON MICROSCOPY TECHNIQUES

There are several techniques that fall under the envelope of 4D ultrafast electron microscopy. While some are capable of single-shot imaging,[2] the majority invoke the concept of single-electron imaging[1] to capture ultrafast dynamics. In fact, since the development of electron microscopes in the 1930s by Ruska and Knoll, it is this concept that made it possible to increase the temporal resolution by 10 orders of magnitude, while maintaining the atomic-scale spatial resolution. In UEM, one optical pulse is used to generate an electron packet and another to initiate the change in the material through optical excitation(s) or by a T-jump. It is the time delay between the electron packet and optical pulse excitation that determines the time scale of the microscope (see Figure 2); the detector response time becomes irrelevant.

The principle behind single-electron imaging is that by allowing only one electron to be emitted from the photocathode at a time there are no electron−electron interactions (space charge effects) in the probing beam that could degrade the coherence and imaging capability of the microscope. In photonic or electronic devices, nearly all dynamical processes are repetitive and do not involve the destruction of the object being probed making single-electron stroboscopic imaging perfectly suited to capture the dynamical processes in these devices. With the idea of single-electron imaging, essentially all variants of transmission electron microscopes[9−11] (see Figure 2), scanning electron microscopes,[12] and low energy point projection electron microscopes[13−15] have been successfully used to image ultrafast dynamics at the nanoscale.

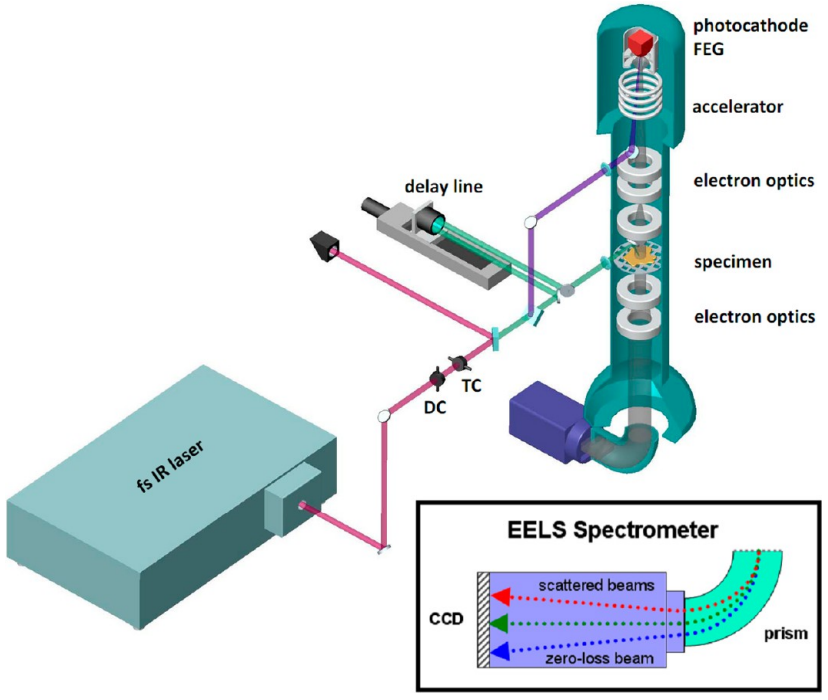

Figure 2. Conceptual design of Caltech's UEM2. A schematic representation of optical, electric, and magnetic components are displayed. The optical pulse train generated from the laser, in this case having a variable pulse width of 200 fs to 10 ps and a variable repetition rate of 200 kHz to 25 MHz, is divided into two parts, after harmonic generation, and guided toward the entries of the designed hybrid electron microscope. The frequency-tripled optical pulses are converted to the corresponding probe electron pulses at the photocathode in the hybrid FEG, whereas the other optical pump beam excites (T-jump or electronic excitation) the specimen with a well-defined time delay with respect to the probe electron beam. The probe electron beam through the specimen can be recorded as an image (normal or filtered, EFTEM), a diffraction pattern, or an EEL spectrum. Figure is adapted with permission from ref 24. Copyright 2009 Elsevier.

DOI: 10.1021/acsphotonics.5b00427
ACS Photonics 2015, 2, 1391−1402

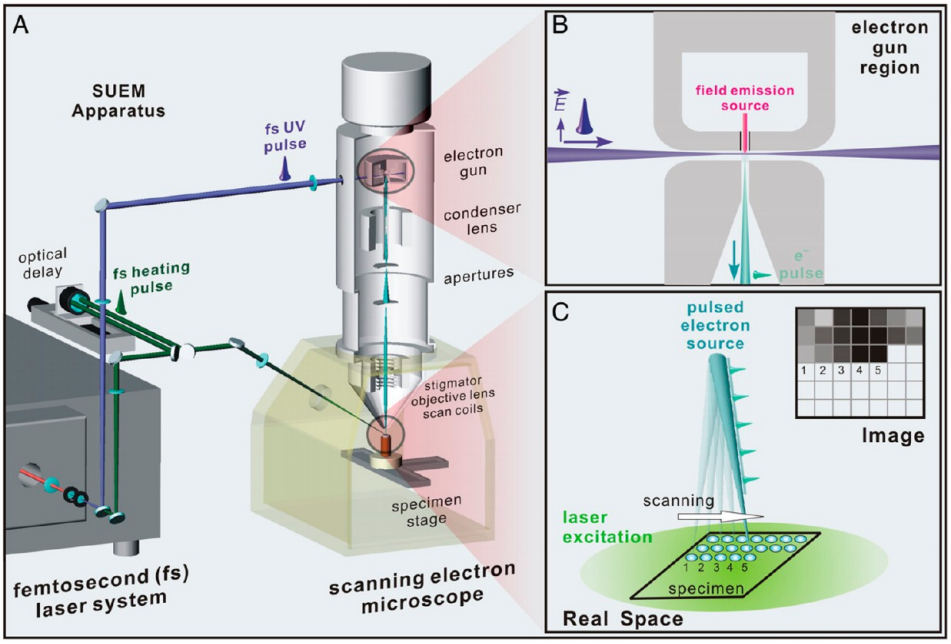

Figure 3. Scanning ultrafast electron microscopy (SUEM), a conceptual schematic. (A) The interface of a femtosecond laser system to a modified SEM. (B) A close-up view of the field-emission region. Side-illumination of the field emitter by fs ultraviolet pulses is used for the electron generation. (C) A close-up view of the probe region and schematic for the pixel-by-pixel image construction. The axis of time is introduced by adjusting the arrival time of the laser excitation pulse at the specimen relative to that of the electron probe pulse using a variable optical delay line. Figure reproduced with permission from ref 12. Copyright 2010 National Academy of Sciences.

The 4D UEM was first developed at the California Institute of Technology[1,2,9,10,16] and is now in many laboratories around the world.[3] With the use of single electrons, the basic functionality of the microscope is identical to that of the conventional microscope, allowing its operation in imaging, diffraction, convergent beam and scanning transmission (STEM) modes.[2] In addition, when combined with an electron energy loss (EEL) detector, energy spectra and energy filtered images can be obtained with nanometer and femtosecond resolutions.

Both scanning UEM (SUEM)[17] (see Figure 3) and low energy point projection UEM[13−15] (see Figure 4) employ single-electron packets to create images. One slight difference is that in the SUEM and low energy point projection UEM a nanometric field emitter[12−15] (1 μm diameter or less) is used so the laser excitation of the cathode needs to occur from the side instead of from the front. The advantage of using the nanometer source size to create the photoelectron packets is that in the SUEM a much smaller scanning probe can be attained and in the point projection UEM the high coherence and small source size allows projection images to be recorded. Normal contrast mechanisms, including the use of secondary electrons and backscattered electrons, can also be used in SUEM, which makes the microscope particularly useful for following electronic changes in nanoscale devices.[12] For low energy point projection UEM both diffraction and imaging (transmission) can be used to follow dynamics, and with the very low energy of the electrons (~100 eV), the microscope is very sensitive to weak electric fields.[18]

These microscopes have successfully imaged laser excited plasmonic near-fields in a variety of nanoparticles and surfaces, followed the electronic and acoustic excitations induced between individual layers of materials, such as graphite, and

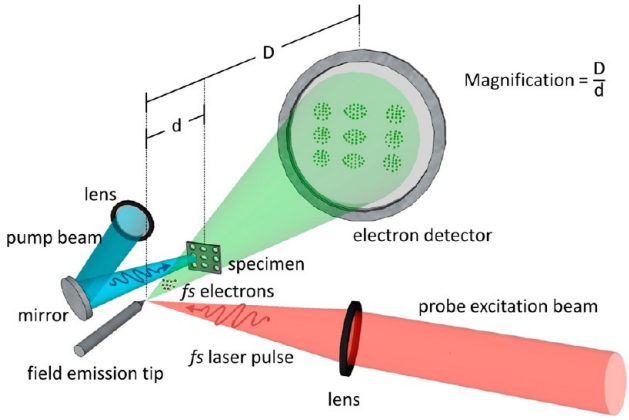

Figure 4. Schematic of the femtosecond photoelectron point projection microscope. The pump beam is used to excite the sample, while the probe beam is used to generate the pulsed electron packets by excitation from a field emission tip. The electron packet is then accelerated to the sample and detected at a distance *D* from the source. Figure reproduced with permission from ref 13. Copyright 2013 AIP Publishing LLC.

have been used to study the wave-particle duality of a plasmonic near field, as discussed below.

CAPTURING BULK AND SURFACE ELECTRON DYNAMICS

Understanding the movement of electrons in materials at the nanoscale is integral to understanding how near-fields and bulk electronic structures couple and evolve. Imaging optically induced currents on nanometer and femtosecond time scales is necessary to create devices which combine electronic/photonic principles. Being able to follow bulk electron dynamics that are internal to the nanostructures with nanometer resolution is a

DOI: 10.1021/acsphotonics.5b00427
ACS Photonics 2015, 2, 1391−1402

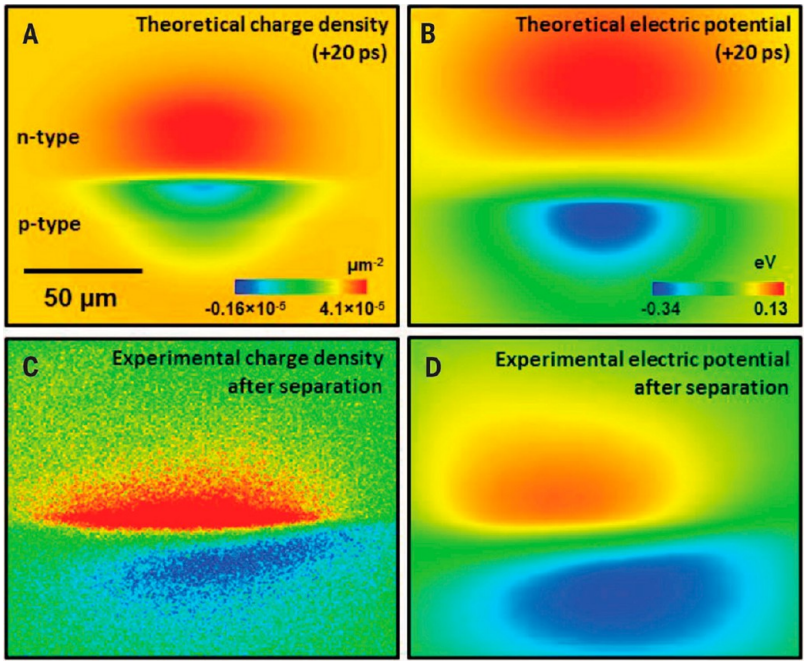

Figure 5. Comparison between experiment and theory. Shown are comparisons between experimental charge density and electric potential and those predicted by the theoretical model following transport. (A) The net theoretical charge density at +20 ps (the asymmetry of excitation is included). The presence of long-range transport, up to tens of micrometers, is evident. The scale of the normalized density shown (-0.16×10^{-5} to 4.1×10^{-5}) when multiplied by N_p, which is 10^9 e−h pairs, gives the actual density. (B) The landscape calculated directly from the Coulomb interactions between separated carriers. The dynamic potential (due to net charge localization) reaches more than 300 meV, which is of the same order of magnitude as the junction potential (0.79 eV). This influences charge localization and carrier recombination. (C) Experimental contrast image of the junction that mirrors charge densities in *n*-type and *p*-type after charge separation. (D) The dynamic potential map calculated directly from the experimental data after charge separation by considering each pixel of the net electrons and holes corresponding to bright and dark contrast and calculating the Coulomb potential. The apparent tilt in the figure is due to the inclined angle of the incident laser beam, which is about 15° with respect to the junction. Figure reproduced with permission from ref 17. Copyright 2015 AAAS.

unique capability of the 4D ultrafast electron microscope. Because the probing electrons can actually penetrate through the material, bulk electronic dynamics can be captured; optical techniques, such as near-field scanning optical microscopy (NSOM) are only able to record surface dynamics and with less resolution. All plasmonic devices rely on this intricate dance between the bulk electronics and the surface near-fields that surround the nanomaterial. By following their dynamics on the femtosecond, and ultimately attosecond time scales, our understanding of how they evolve will greatly enhance the understanding and capabilities of future plasmonic devices. Following electronic dynamics can be accomplished using SUEM, low energy UEM, and femtosecond electron energy loss spectroscopy (FEELS).

SCANNING ULTRAFAST ELECTRON MICROSCOPY

A recent study[17] using SUEM was able to follow the dynamics of charge carriers in a *p*−*n* junction and was accomplished by taking pump−probe images of a wafer containing a *p*−*n* junction, see Figure 5. After optically exciting the *p*−*n* junction with femtosecond laser pulses (fluences on the order of ∼1 mJ/cm^2) electrons are promoted to the conduction band. The junction field then causes a separation of holes (h) and electrons (e), which each drift in opposite directions. However, the rapid transport of carriers found experimentally to occur over tens of micrometers in ∼100 ps cannot be understood by the drift-diffusion model,[19] which is usually very successful in describing charge movement in the vicinity of the junction. Instead a model is employed which takes into account the high initial energy of the carriers and includes their energy dampening due to lattice phonon interactions.[17] This study found an unexpected ballistic motion of the carriers which could only be captured with high spatial and temporal resolution, making it a perfect example of how 4D UEM enables the mapping of surface electron motion at the nanoscale.

In addition to the previous study, one can imagine a number of experiments where the SUEM technique would provide useful and unique insight into a nanophotonic circuit. For example, a recent paper describing a graphene-silicon hybrid integrated circuit used a conventional SEM to investigate the ability of a circuit to act as a local and nonlocal switch for light.[20] In their study the authors were able to follow the light-controlled modulation with millisecond temporal resolution. However, for photonic circuits to be useful, switching has to be done at much higher rates, which would require greater temporal resolution than is accessible in a conventional SEM. By using SUEM, these same circuits could be examined, and by following the dynamical motion of the charge carriers, it would be possible to image how they move in real time. This information is the key to creating photonic circuits that switch faster, more efficient and are compact.

While the secondary electrons in SUEM are sensitive to the dynamics of surface fields, another promising technique would be to combine SUEM with a cathodoluminescence detector. Cathodoluminescence has already been shown to work in a femtosecond pulsed SEM using the electron beam to excite the plasmons.[21] By installing a cathodoluminescence detector on a

DOI: 10.1021/acsphotonics.5b00427
ACS Photonics 2015, 2, 1391−1402

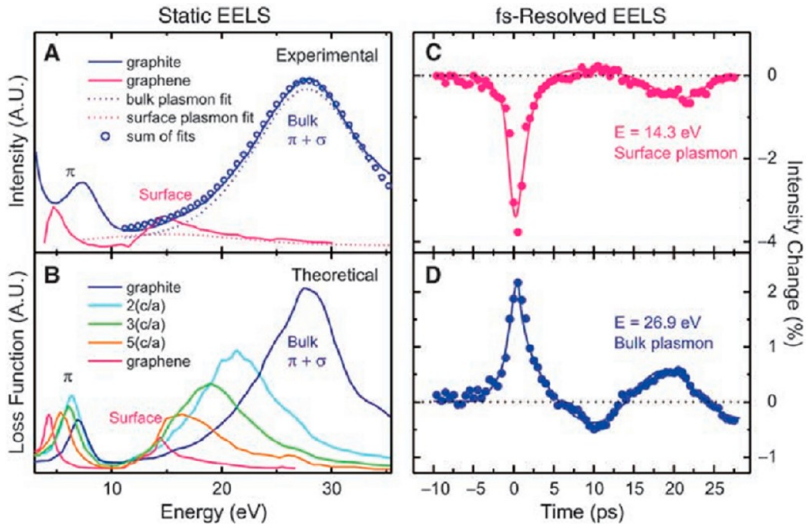

Figure 6. Static and femtosecond-resolved EELS of graphite. (A) UEM-obtained experimental spectrum of graphite; for comparison with the spectrum of graphene, see ref 72. (B) Simulated spectrum for natural graphite, together with the calculated spectra obtained for expanded *c*-axis structures, with the separation being twice, three times, and five times as large as the native one.[73] The theoretical spectrum of graphene is also displayed.[72] (C, D) Peak intensity changes of surface (C) and bulk (D) plasmons as a function of time. Solid lines are guide to the eyes. The increase in intensity for the bulk corresponds to a decrease in intensity for the surface plasmon (i.e., nearly out of phase). This figure is reproduced with permission from ref 25. Copyright 2009 AAAS.

SUEM, the photons emitted when optically excited plasmons decay into photons can be captured with femtosecond resolution. This would provide information on the surface near-field dynamics of plasmonic relevant devices, and when combined with secondary electron detection in the SUEM, an enhanced picture of the surface field dynamics would become possible.

LOW ENERGY POINT PROJECTION ULTRAFAST ELECTRON MICROSCOPY

Besides the proven ability of the SUEM to follow carrier dynamics, the recent development of low energy ultrafast point projection electron microscopy is also suitable for imaging surface near-field dynamics. Low energy (~100 eV) electrons are easily deflected by electric fields when compared to the higher energies (~10−300 keV) found in conventional SEM and TEM. While these deflections would normally be thought of as detrimental to image formation, in point projection microscopy it simply means that the microscope can image the effects of the weak electric fields. By extending this technique to the 4D regime, optically excited transient surface fields of nanostructures can be measured with ultrafast temporal resolution.[18]

Recent studies showed that such a microscope can be used to follow the ultrafast melting of a polymer/graphene bilayer system. Due to the very low electron energies, graphene is the ultimate substrate for transmission studies with this type of device. In one method of preparation, poly(methyl methacrylate) or PMMA is used to functionalize the graphene for transfer to different substrates. Since this PMMA is particularly difficult to remove from the graphene after transfer,[22] it was an ideal first system to study. Using low energy UEM in diffraction the ultrafast melting and then resolidification of the PMMA on the graphene layers was captured.[14] What was found was that the 800 nm femtosecond laser pump pulses primarily deposit energy in the graphene, which happens within the laser pulse duration. The energy that is absorbed by the graphene takes a much longer time, ~50 ps, to equilibrate its temperature with the PMMA layer. After ~100 ps, the PMMA loses its crystallinity, followed by an increase in the PMMA chain spacing and a relaxation into the amorphous structural phase.[14] While this study focused more on structural dynamics, the fact that they were able to follow dynamics with picosecond temporal resolution using ~500 eV electrons showed the sensitivity of the microscope. In future experiments, this microscope will be particularly useful in studying surface near-field excitations in nanoparticles.[13] A more recent study showed that the resolution of the microscope could be extended to below ~100 fs while achieving a 10 nm spatial resolution.[15]

One advantage of the low energy electron point projection technique is the very compact distance between the field emission tip and the specimen being imaged. This can prevent a primary cause of electron pulse broadening,[13,23] which is dispersion. Dispersion happens to the electron pulse because it is made up of electrons with different energies and, hence, different velocities. The energy spread is typically 1 eV for most electron sources, which is enough to prevent pulse durations of less than several hundred femtoseconds to be delivered to the specimen in a UEM based on a conventional electron microscope design. However, in the point projection UEM, the fact that the electron source is only micrometers away from the specimen being imaged does not allow any time for the electron pulse to disperse. By using shorter laser pulses to create the electron packets, it is reasonable to think that temporal resolutions on the tens of femtoseconds or possibly better could be achieved in these geometries.[13,23] By reaching temporal resolutions on the order of tens of femtoseconds or less, dynamical imaging of optically induced plasmons will become achievable with nanometer spatial resolution.

ENERGY SPECTROSCOPY IN 4D UEM

In femtosecond electron energy loss spectroscopy (FEELS),[24,25] the bulk electronic structure of nanoscale materials can be followed by tracking the changes in the low energy loss spectra. This technique works by having a laser

DOI: 10.1021/acsphotonics.5b00427
ACS Photonics 2015, 2, 1391−1402

pulse excite a nanoscale specimen, and the probing electron pulse subsequently interacts with the specimen. By varying the delay time between the excitation laser pulse and the probe electron pulse and recording EEL spectra or energy filtered images at each delay point, the dynamical bulk and surface electronic structure of the specimen can be captured. This technique was successfully used to follow chemical bond dynamics in a thin film of graphite. As shown in Figure 6, the spectra acquired at each time point in the scan is directly related to the surface and bulk plasmons in graphite. When examining the spectra, the intensity in the energy loss region related to the surface plasmon decreases in ∼200 fs, while the bulk plasmon intensity increases during the same time. This behavior is explained by the following:[25] For the first ∼100 fs, the electronic structure is pushed out of equilibrium due to the photoinduced increase in the carrier temperature. For the next ∼500 fs, the electronic structure relaxes back to equilibrium through optical phonon emission.[26] The phonons primarily cause in-plane vibrations of the graphene atoms, which enables a different stacking of the graphene layers and a contraction along the *c*-axis in the ∼1−3 ps time scale.[26] This structural contraction (and the following oscillations in the *c*-axis spacing) causes distortions in the bulk and surface electronic structure, which can be followed in the detected EEL spectra. The behavior of photoexcited graphite to initially contract before expansion can only be captured with ultrafast techniques, and this experiment utilizing FEELS to image this behavior is directly supported by other ultrafast imaging and diffraction techniques.[27−29]

This study using FEELS is particularly relevant for future photonics circuits, as graphene is increasingly being used in plasmonic-based devices,[30] and as switching speeds in these devices increase, how the electronic structure of these materials behave on the ultrafast time scale will become increasingly important. Other 4D UEM techniques have not only been able to observe the electronic structural changes in graphite, but have also shown sensitivity to near-fields at the edges of single layers of graphene.[31] Spectroscopic *imaging* in the femtosecond regime with the FEELS techniques has not yet been attempted; however, it promises to be a powerful technique able to image the motion of different plasmons in nanoparticles. By selecting only the electrons corresponding to a particular range of loss energies, plasmons can be followed spatially as they evolve after the laser pump excitation pulse. The potential applications of FEELS and the evolution of EELS over half a century can be found in the insightful perspective by Thomas.[32] The perspective details how the FEELS technique is a competitive alternative to following ultrafast electronic structures in solids that until recently was only possible using a synchrotron or free-electron laser.

While current UEM instrument resolutions are on the nanometer spatial scale, there is room for improvement to the temporal resolution. With the ∼100 fs to ∼1 ps resolutions currently available,[1] much of the dynamics of the electronic motion is lost. As resolution limits are extended to 10 fs or even 1 fs, it will become possible to capture the motion of plasmons as they are being excited. Ultimately, capturing the movement of the electrons in materials as they are experiencing forces due to the electric field of the excitation light will allow details of how light and electrons couple in complicated nanodevices.

IMAGING CONFINED LIGHT: THE PINEM CONCEPT AND TECHNIQUE

Imaging near-field enhancements at nanoscale interfaces has primarily been the domain of optical microscopy, which would include stochastic optical reconstruction microscopy[33] (STORM), near-field scanning optical microscopy,[34] and apertureless NSOM[35] (ANSOM), to mention a few. While there are electron microscopy techniques such as cathodoluminesence (CL) done in either a SEM,[21] STEM,[36] or STEM combined with EELS,[37] these techniques rely on electron beam excitation of the plasmons in the nanostructure. In the former optical methods, the spatiotemporal resolution cannot reach that of UEM, and in the latter electron-based excitation, there is little control over the excitation of the material.

Recently, with the development of 4D UEM, a new method dubbed photon-induced near-field electron microscopy (PINEM)[38] has been realized. In PINEM, a femtosecond laser pulse directly excites the plasmons in a nanoparticle or at an interface. During the laser excitation, the near-field that surrounds the interface facilitates the direct coupling of the imaging electrons with photons in the laser excitation pulse[39] (see Figure 7A). The result is that the imaging electrons (with energies typically on the order of 200 keV) absorb/emit integer numbers of photons. Unlike traditional EELS, which can detect the zero loss beam and electrons that have lost energy due to inelastic collisions, in PINEM, electrons can gain energy by absorbing photons. The absorption/emission can be detected by recording EEL spectra of the electron beam (see Figure 7B), which captures the electrons having absorbed photons or gaining energy and those electrons emitting photons resulting in a loss of energy. In the spectra, peaks appear as sidebands to the zero loss peak spaced by the photon energy of the pump laser pulse. When an energy filtered image is constructed using only the energy gained electrons, the excited near-field that surrounds the nanostructure is fully realized.

The PINEM technique has been used to image the near fields surrounding metallic nanowires,[11,38] carbon nanotubes,[38] nanoparticles and their entanglement,[40−42] stained cells,[43] and protein vesicles,[43] to list a few (see Figure 8). In addition, PINEM can also be combined with scanning TEM to get point specific information on the surrounding near-field.[40]

The PINEM technique, in a similar manner to SUEM, is useful for the investigation of photonics circuits that are used as the building blocks for plasmonic devices. In the previous example, where SUEM could follow a graphene−silicon hybrid integrated circuit to investigate the ability of a circuit to act as a local and nonlocal switch for light,[20] a PINEM experiment done on this same device would be able to track the induced near-fields, and FEELS could be used to follow the bulk transient electronic excitations. Combining this dynamical plasmon information with that captured in the SUEM would give a detailed picture of how such a device operates, both electronically and optically.

VARIANTS OF PINEM AND THEORY

In addition to imaging the near-field surrounding materials of various composition and shape, the PINEM technique has been used to study the wave-particle duality of near-field light.[44] A recent study was able to simultaneously show the quantization of the near-field and its interference pattern, all in a single image. In PINEM, the imaging electrons carry all the information on their interaction with the specimen in their

DOI: 10.1021/acsphotonics.5b00427
ACS Photonics 2015, 2, 1391−1402

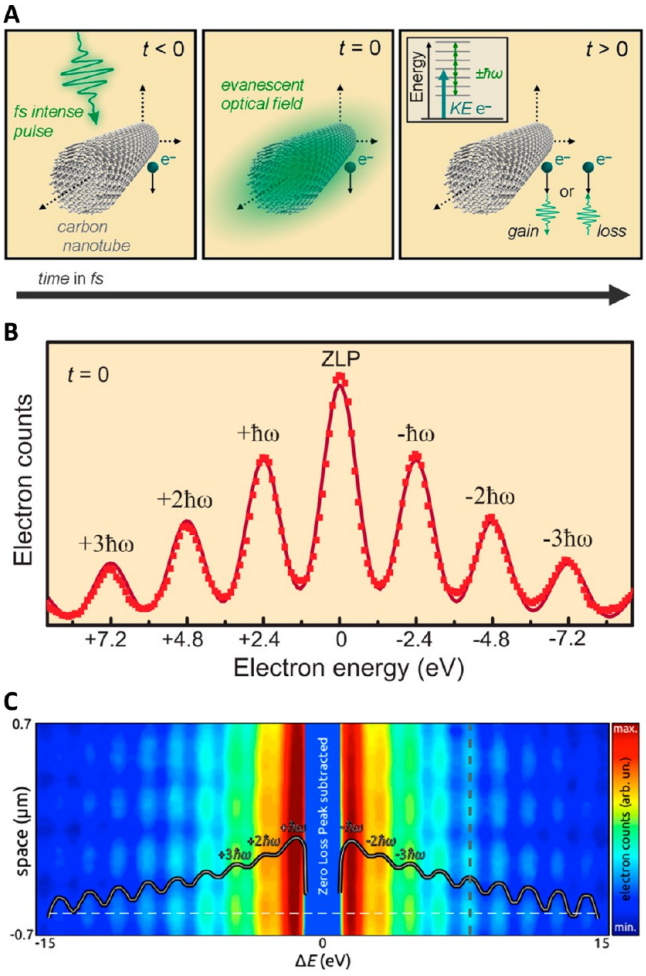

Figure 7. PINEM physical description, EEL spectra showing quantized photon exchange, and energy-space map of Fabry–Perot resonance. (A) Left frame showing when the electron packet arrives at the nanotube before the femtosecond laser pulse ($t < 0$); no spatiotemporal overlap has yet occurred. Middle frame showing the precise moment at $t = 0$ when the electron packet, femtosecond laser pulse, and evanescent field are at maximum overlap at the carbon nanotube. Right frame shows the process during and immediately after the interaction ($t > 0$) when the electron gains/loses energy equal to integer multiples of femtosecond laser photons. Inset: the possible final energies in the continuum due to the free–free transitions between the imaging electron and the photons in the femtosecond laser pulse. KE: kinetic energy. Figure adapted with permission from ref 38. Copyright 2009 Nature Publishing Group. (B) PINEM electron energy spectrum obtained at $t = 0$. The energy is given in reference to the loss/gain of photon quanta by the electrons with respect to the zero-loss energy. Figure adapted with permission from ref 38. Copyright 2009 Nature Publishing Group. (C) The experimentally obtained energy-space image, taken on a selected section of a photoexcited nanowire (4.6 mm length, ~61 nm radius, 800 nm excitation, $\phi = 0$, $\Delta t = 0$ ps). The horizontal axis shows the quantized energy dependence of near-field and the vertical axis shows the interferometric spatial distribution of the SPP field. A Gaussian-fitted ZLP peak was subtracted, and the intensity (electron counts) is mapped on a logarithmic scale in both the image and the spectrum to enhance the contrast. Figure adapted with permission from ref 44. Copyright 2015 Nature Publishing Group.

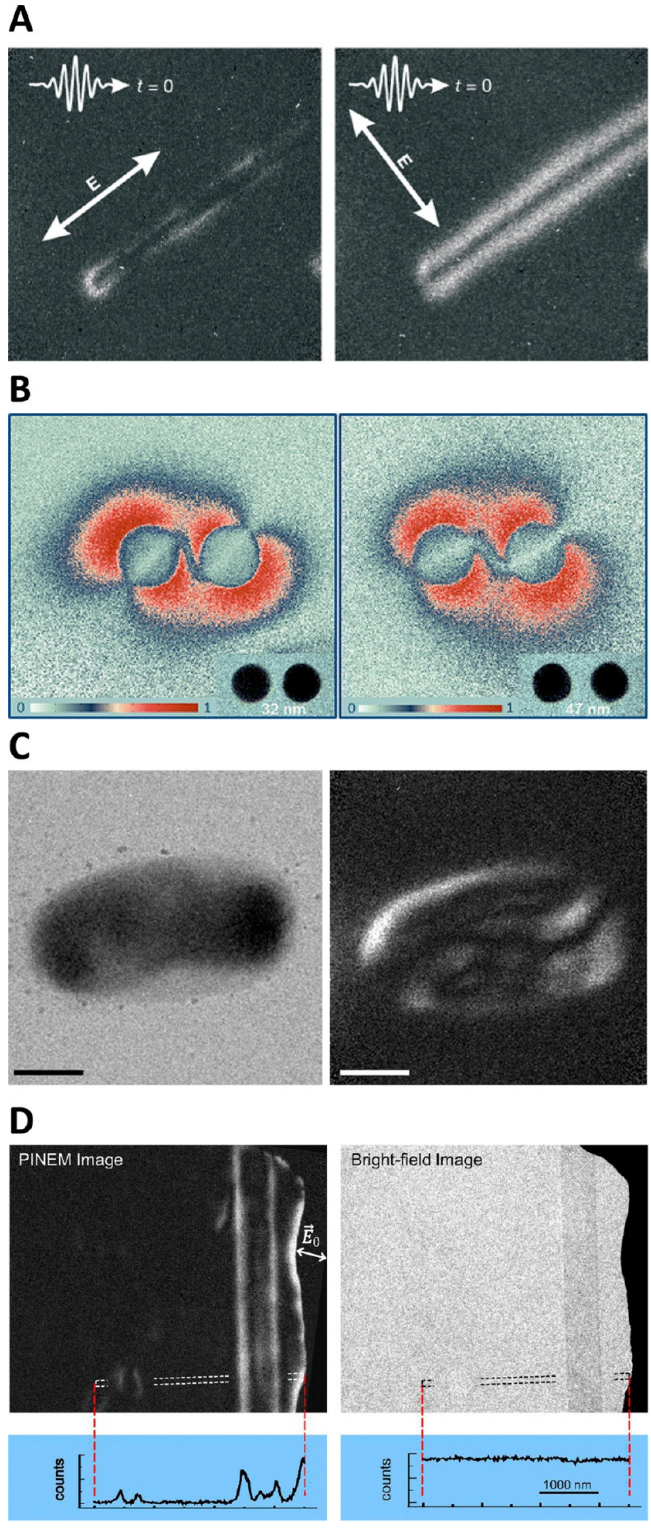

Figure 8. PINEM of different nanostructures. (A) Two images taken when the *E*-field polarization of the femtosecond laser pulse is parallel to (left image) and perpendicular to (right image) the long-axis of the carbon nanotube. Both polarization frames were taken at $t = 0$, when the interaction between electrons, photons, and the evanescent field is at a maximum. Figure taken with permission from ref 38. Copyright 2009 Nature Publishing Group. (B) Shown are the near-fields of a nanoparticle pair with an edge-to-edge distance of 32 (left) and 47 nm (right) with false-color mapping. When the separation between the particles is reduced to 32 or 47 nm, a "channel" is formed between them, as seen in the left and right panels. The bright field images of the

spatial and energy distributions. By recording a spectrum, the energy exchange of individual quanta between the electron and the photons in the pump laser beam can be captured. This is

DOI: 10.1021/acsphotonics.5b00427
ACS Photonics 2015, 2, 1391–1402

Figure 8. continued

nanoparticle pairs (obtained in UEM) are shown in the inset at the bottom right of each of the left right panels; PINEM images are displayed at a higher magnification than the bright-field UEM images in order to emphasize the near-fields surrounding the particles. The false-color bars are shown at the bottom left of each panel; white indicates the lowest intensity and red the highest. Polarization of the exciting laser field is at 45° counterclockwise for both panels. Figure taken with permission from ref 42. Copyright 2012 American Chemical Society. (C) Bright-field TEM and PINEM images of a whole unstained and unfixed *E. coli* cell. Both images were obtained at a magnification of 19000×. The PINEM image was filtered for noise removal (scale bars: 500 nm). The figure is taken with permission from ref 43. Copyright 2010 National Academy of Sciences. (D) Comparison of PINEM data and TEM bright-field data for the same area. (Upper) Images: The graphite specimen is bounded on the right by a copper grid bar. The dotted line boxes indicate the image area from which the profiles below were extracted. (Lower) Average image intensity profiles of the boxed area in the images. Intensities were averaged over the 10 pixel width of the boxes. The scale bar at lower right applies to the entire panel D. Figure 8D is, with permission, from ref 74. Copyright 2013 National Academy of Sciences.

accomplished by collapsing (or focusing) the spatial pattern and dispersing the electrons on the detector according to their energy. This distribution is then displayed as a 1D plot of the energy spectrum of the electron beam. The same electron detector can also be used to produce a 2D energy filtered image, where a slit is used to block out all electrons, except those that have gained energy. These energy gained electrons are then used to make a 2D spatial image that is recorded by the detector. The filtered image gives a map of where on the specimen photons were absorbed. There is a third possibility, dubbed energy-space mapping,[44] where one axis of the detector corresponds to the energy of the electrons, and the second axis corresponds to a single spatial dimension. This is accomplished by using the energy filter to focus a single spatial axis (for example, the *x*-coordinate) while projecting the *y*-coordinate spatial information on the vertical detector axis, see Figure 9. At

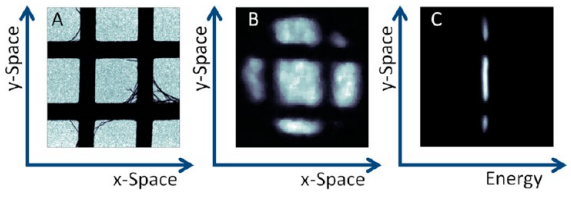

Figure 9. Energy-space imaging in PINEM. (A) Bright field image of a TEM grid. (B) The same TEM grid as imaged with GATAN spectrometer, while unfocused in the *x*-direction. (C) Figure showing the same grid when focused in spectroscopy mode. The vertical or *y*-direction still shows the horizontal grid bars after focusing in the *x*-direction. While the electrons are focused in the *x*-direction, the electrons are dispersed according to energy on the horizontal detector axis. Data were obtained by Luca Piazza.

the same time, the energy spectrum is dispersed on the horizontal axis of the detector, which results in an energy-space map where the detected image contains spectroscopic information along one axis (horizontal) and spatial information along the other axis (vertical).

By choosing an appropriately aligned nanowire (with its long axis oriented parallel to the vertical detector axis), laser excited Fabry–Perot type resonances can be seen along its length that show the spatial interference pattern (wave-like behavior of the near-field), see Figure 7C. In the same image, the quantized photon absorption/emission energy sidebands or the quantized energy exchanged between the imaging electron and the quantized near-field can also be seen (Figure 7C). This study shows the reach of 4D UEM to not only expand our understanding of structural, electronic, and near-field dynamics, but also to probe fundamental quantum problems.

In another study, the interaction that occurs between light and electrons in PINEM was shown to be a coherent process.[45] This was accomplished by following the population of the sidebands created by electrons emitting/absorbing photons as a function of the pump laser beam intensity. A signature of the energy exchange process being coherent is the extinction of the primary electron beam energy as compared to the sidebands. This primary electron beam energy extinction cannot be explained classically. The suppression of the primary beam energy was previously predicted in two separate theoretical studies[39,46] along with experimental data, showing this behavior in the PINEM spectra from a silver wire bundle.[39] The coherent behavior of the PINEM mechanism is of fundamental interest as a method to coherently control electrons in the microscope through optical means and of practical interest because it provides an alternate route for the creation of attosecond electron pulses.[39,45,49,48]

DISCUSSION AND OUTLOOKS

Attosecond Electron Microscopy. While attosecond time resolution in UEM has not yet been achieved experimentally, there have been several reports outlining new methods for pushing the resolution limits.[47,48] Few-femtosecond phase stabilized lasers are now commercially available, but the main hurdle in improving the temporal resolution of UEM is to decrease the duration of the electron pulse below the hundreds of femtosecond regime. Even in the single-electron regime, where space charge is minimalized or absent, electron pulse dispersion is still present. Several methods have been proposed to manipulate the electron pulses in a UEM to further push the resolution limits of the microscope and correct for the dispersion. One well-known technique is that of microwave compression[49] of electron pulses, which has recently been applied in femtosecond electron diffraction setups.[50]

A more promising method for compression directly to the attosecond domain involves the creation of "temporal lenses" made by ultrashort laser pulses.[47,48] The technique relies on the ponderomotive force (or ponderomotive potential) that influences electrons when they encounter an intense electromagnetic field. To create trains of attosecond electron pulses, appropriate optical intensity patterns have to be synchronized with the electron pulse. This is done by using counter propagating laser pulses to create a standing optical wave that must be both spatially and temporally overlapped with the femtosecond electron pulse to get the desired compression. To make the standing wave in the rest frame of the electron pulse, the two counter propagating electromagnetic waves must have different frequencies[47] or be angled appropriately;[48] see Figure 10. The standing wave that appears in the rest frame of the traveling electron pulse introduces a series of high and low intensity regions, and in this periodic potential each of the individual ponderomotive potential "wells" cause a compression of the local portion of the electron pulse that encounters it.[48] After interaction with the optical potential well, the electrons that have encountered steep intensity gradients get sped up or

DOI: 10.1021/acsphotonics.5b00427
ACS Photonics 2015, 2, 1391–1402

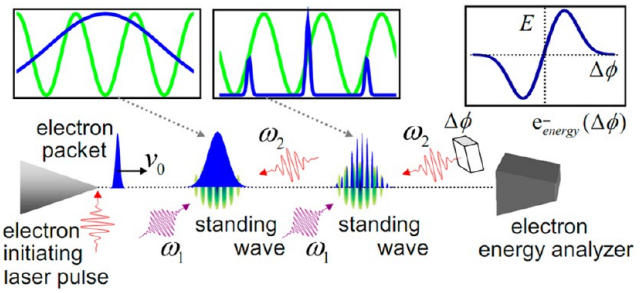

Figure 10. Schemes for creating and measuring attosecond compressed electron packets. To measure the duration of the attosecond pulses, a second copropagating standing wave is made to coincide with the electron pulse at the focal position. Instead of using a temporal delay, a phase shift, $\Delta\varphi$, is introduced into one of the laser pulses that creates the probing standing wave. By varying this phase shift, the nodes of the standing wave shift position. The average electron energy can thus be plotted vs this phase shift. As the electron pulses become shorter than the period of the standing wave the change in the average energy will increase. To use the attosecond electron pulse train as a probing beam in a UEM, the specimen would need to positioned where the second standing wave appears in the figure. Figure taken with permission from ref 48. Copyright 2009 National Academy of Sciences.

slowed down, depending on their position in the potential. After additional propagation, the electron pulse self-compresses into a train of attosecond pulses, with the pulse train spacing equal to the periodicity of the optical standing wave. By placing the compression potential at an appropriate distance before the specimen, the pulse will be maximally compressed when encountering the system under study.

A UEM equipped with this optical electron compression device would be able to deliver the train of attosecond electron pulses onto a nanostructured specimen. When a phase-stabilized femtosecond laser pulse that has a wavelength matched to the periodicity of the attosecond electron pulse is used to pump the specimen, it will be possible to follow subcycle dynamics in a variety of materials.[48] The relative delay between the probe attosecond electron pulse train and the phase-stabilized pump laser pulse can be precisely controlled by using refractive optical elements, such as glass wedges to control the relative phase between the electron and laser pulses.[47] It might also be possible to use attosecond UV pulses,[51] which are created through high harmonic generation, to pump the electron dynamics in the specimen. With control in the attosecond time domain, it will become possible to examine the dynamics of bulk electronic and surface near-fields in arbitrary nanophotonic specimens on the time scales of excitation and decay at the interfaces. However, the tens of eV energy width of the pump process must be considered, as dictated by the uncertainty principle, for the probing of the dynamics.

Electron Vortex Beams in UEM. Recently, there has been much interest in both optical and electron vortex beams, due to their unique properties, which allow them to carry orbital angular momentum (OAM). In optical beams, the ability to carry OAM has led to proposals to vastly increased bandwidth in optical communications[52] and lead to faster communications using telecommunications optics. OAM optical beams with their additional quantum number, m, enable more information to be carried, due to the additional degree of freedom. To implement these optical beams in communication setups, nano-optical devices capable of coupling this light to electronics need to be developed.

UEM with PINEM could provide a unique insight into how such nano-optical devices operate on the ultrafast time scale. By excitation of these devices with an optical pump pulse containing OAM, the response of the plasmonic circuit can be followed. This would bring a better understanding about how "twisted" light can be both detected and emitted in a nanoplasmonic circuit.

Conversely, by combining electron beams carrying OAM with UEM will provide increased sensitivity when measuring the dynamics of magnetic structures[53] and chiral plasmonic structures.[54] By examining the electron energy spectra as a function of the electron beam OAM, recent demonstration experiments[55] have shown the ability of vortex electron beams to study chiral structures in transmission electron microscopes. It has been predicted[54] and experimentally confirmed[55,56] that EEL spectra should show large dichroism with respect to the OAM carried by the imaging electron beam for structures with a different chirality. The dichroic coupling between electron beams carrying left- and right-handed OAM with materials is caused by a combination of structural dimensions, orientation and the plasmons that have been excited. This dichroic coupling leads to large asymmetries between EEL spectra taken using the left and right electron beams, and when combined with PINEM or FEELS in a 4D UEM, the dynamics of the coupling of OAM light to nanomaterials will be revealed. To carry out these studies, an electron vortex beam has to be created with an ultrashort duration. One recent study suggested the use of Kapitza–Dirac scattering of electrons with photons carrying OAM, to produce beams with arbitrary amounts of OAM and durations in the femtosecond regime.[57]

PINEM for Biological Imaging and Dynamical Imaging of Biophotonic Structures. Typically, electron microscopy of biological material is done using phase-contrast imaging of cryo-specimens.[58] While this technique is extremely powerful, it has strict requirements for the coherence of the electron beam, it requires the use of cryo-microscopy stages, and it requires some thousands of images to be captured to reconstruct the original biomaterial structure. PINEM imaging, which uses only the electrons that have absorbed photons to create an energy filtered image, is a completely different contrast mechanism from that of "phase" contrast imaging. For phase contrast, high coherence is needed because the image projected on the microscope detector is actually an interference pattern between the part of the electron wave that has scattered from the specimen and the unscattered portion of the wave.[59] In PINEM, the image is not made through electron interference, but instead is made by simply selecting electrons that have gained energy through photon absorption.[38] This PINEM contrast has already been shown to work with protein vesicles and stained cells,[43] and the resolution is determined by the coherence length of the near-field.[39] By combining PINEM with liquid flow cell specimen holders,[60] biomolecules that have been tagged with nanoparticles,[61] which interact strongly with the pump light, may provide a method for dynamical imaging of live cells in real time.

UEM may also be useful in the characterization of a variety of biosensors, including those based on photonic waveguides[62] and those that use surface plasmon resonances[63] (SPR) to increase chemical sensitivity. These biosensors are routinely used to help identify certain biomaterials that are associated with specific diseases.[64] These devices are commercially viable;

DOI: 10.1021/acsphotonics.5b00427
ACS Photonics 2015, 2, 1391–1402

with one example being those used in the measurement of blood glucose levels.[65] Current sensors are based on optical detection and use the SPRs to increase signal or to mark particular biomaterials for detection.

To make these biosensors more useful, they have to be miniaturized and contained in a small electronic "chip".[66] Ultimately more biosensors should be included in smaller volumes for ease of use in the clinical setting. With UEM, these chips that rely heavily on SPR, can be characterized with PINEM. Typically, numerical simulations are relied on to predict the behavior of the SPRs and how they interact with molecules,[67] but experimental visualization of the near-fields and their dynamics will aid in optimization of the efficiency and control of the biosensor.

PINEM and the New Advances. Future advances in 4D electron microscopy and, in particular, the ability of this developing technique to follow optical excitations at the nanoscale depends heavily on the electron source. To gain better temporal resolution, increased spatial resolution, and decreased image acquisition times, brighter pulsed electron sources are needed. There are several techniques that hold the promise of creating shorter electron pulses while also providing increased brightness. The first of these that has already been implemented relies on photo-assisted field emission,[17,45] which greatly increases the sources brightness due to their nanoscale emission site sizes and, in principle, can emit electron pulses with attosecond durations.[68,69] Another very promising technique is to create ultrashort electron pulses from field emission tips through surface plasmon excitation.[70] In this source, the tip apex is not directly hit by the excitation laser pulse, but instead, laser-induced plasmons are focused toward the tip apex, causing electron emission. This technique avoids direct excitation of the tip while still producing ultrashort electron pulses and will find applications in both conventional TEM-based UEMs and has been demonstrated in a point projection low energy UEM.[70]

A recently developed,[71] ultrafast, multiple-cathode source has been used to enable multiple images of the same microscopic dynamic process to be captured. This source allows both reversible and irreversible processes to be followed by creating multiple electron pulses with the same cathode excitation laser beam. Because the separate cathodes are spatially separated, the image (or diffraction) patterns they create appear spatially separated on the detector. The spatial separation of the cathodes also creates a temporal delay between the electron pulses if one cathode is placed behind the other. In principle, this source enables snapshots of dynamics to be captured of irreversible ultrafast phenomena and will also be useful in studies involving reversible nano-optical dynamics.

Very recently at Caltech, we have developed a new variant of PINEM, which constitutes a breakthrough in electron pulse imaging. In all of the above experiments conducted in 4D electron microscopy only one optical pulse is used to initiate the change in the nanostructure.

In a recent report,[75] we have used two optical pulses for the excitation and one electron pulse for probing. The result of this pulse sequence led to the concept of "photon gating" of electron pulses as shown in Figure 11, resulting in an electron pulse width limited only by its optical gate pulse width. A picosecond electron pulse can now be reduced to the femtosecond optical pulse width of the excitation. This is a very important advance with the potential for many applications in materials visualized in space and time.

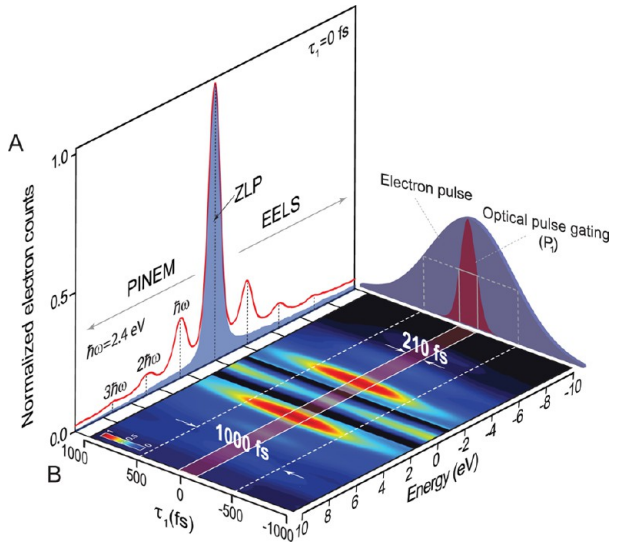

Figure 11. Ultrafast "optical gating" using 3-pulse sequence in photon-induced near field electron microscopy (PINEM). (A) PINEM spectrum at τ_1 = 0 fs, which consists of discrete peaks on the higher and lower energy sides of the zero loss peak (ZLP) separated by multiple photon-energy quanta (~2.4 eV). The shaded curve presents the normalized ZLP measured at τ_1 = 1000 fs. (B) PINEM spectrogram of photon-electron coupling of the first optical and electron pulse as a function of the first optical pulse delay (τ_1). The ZLP area between −1.5 eV and 1.5 eV has been reduced for visualization of the adjacent discrete peaks. Optical gating is clearly manifested in the narrow red strip corresponding to the width of the optical pulse (210 ± 35 fs) shown in red in the vertical plane at right, which is superimposed on the ultrafast electron pulse (1000 fs) in blue. The material studied is vanadium dioxide nanoparticles which undergo metal-to-insulator phase transition when appropriately excited.

CONCLUSION

Ultimately near-fields and dynamics of the electron carriers in materials cannot be decoupled. Being able to image them both with 4D UEM makes it the tool of choice for nanophotonics and plasmonics; their ultrafast dynamics are ideal for stroboscopic imaging with the single-electron concept being invoked. With the capability of SUEM and low-energy UEM to follow the surface electric field, PINEM to exchange quantized numbers of photons with the coupled near-field, and FEELS to image the bulk and surface electronic structure, a complete picture of the underlying dynamics can be captured in a wide variety of photonic systems. This is besides the powerful structural dynamics, and the variant techniques of tomography, convergent-beam imaging, single particle, and core-atom detection, which has already been realized in 4D UEM.[1−3]

AUTHOR INFORMATION

Corresponding Author

*E-mail: zewail@caltech.edu.

Notes

The authors declare no competing financial interest.

REFERENCES

(1) Zewail, A. H. Four-Dimensional Electron Microscopy. *Science* **2010**, *328*, 187−193.

(2) Zewail, A. H.; Thomas, J. M. *4D Electron Microscopy: Imaging in Space and Time*; Imperial College Press: London, 2010.

(3) Zewail, A. H. *4D Visualization of Matter: Recent Collected Works of Ahmed H Zewail*; Imperial College Press: London, 2014.

DOI: 10.1021/acsphotonics.5b00427
ACS Photonics 2015, 2, 1391−1402

(4) Vasa, P.; Ropers, C.; Pomraenke, R.; Lienau, C. Ultra-fast nano-optics. *Laser Photonics Rev.* **2009**, *3*, 483−507.
(5) Atwater, H. A. The promise of plasmonics. *Sci. Am.* **2007**, *296*, 56.
(6) Zhu, Y.; Duerr, H. The future of electron microscopy. *Phys. Today* **2015**, *68*, 32−38.
(7) Brabec, T.; Krausz, F. Intense few-cycle laser fields: Frontiers of nonlinear optics. *Rev. Mod. Phys.* **2000**, *72*, 545−591.
(8) Kim, J. S.; LaGrange, T.; Reed, B. W.; Taheri, M. L.; Armstrong, M. R.; King, W. E.; Browning, N. D.; Campbell, G. H. Imaging of Transient Structures Using Nanosecond in Situ TEM. *Science* **2008**, *321*, 1472−1475.
(9) Park, H. S.; Baskin, J. S.; Kwon, O.-H.; Zewail, A. H. Atomic-Scale Imaging in Real and Energy Space Developed in Ultrafast Electron Microscopy. *Nano Lett.* **2007**, *7*, 2545.
(10) Lobastov, V. A.; Srinivasan, R.; Zewail, A. H. Four-dimensional ultrafast electron microscopy. *Proc. Natl. Acad. Sci. U. S. A.* **2005**, *102*, 7069.
(11) Piazza, L.; Masiel, D. J.; LaGrange, T.; Reed, B. W.; Barwick, B.; Carbone, F. Design and implementation of a fs-resolved transmission electron microscope based on thermionic gun technology. *Chem. Phys.* **2013**, *423*, 79−84.
(12) Yang, D. S.; Mohammed, O. F.; Zewail, A. H. Scanning ultrafast electron microscopy. *Proc. Natl. Acad. Sci. U. S. A.* **2010**, *107*, 14993−14998.
(13) Quinonez, E.; Handali, J.; Barwick, B. Femtosecond photoelectron point projection microscope. *Rev. Sci. Instrum.* **2013**, *84*, 103710.
(14) Gulde, M.; Schweda, S.; Storeck, G.; Maiti, M.; Yu, H. K.; Wodtke, A. M.; Schäfer, S.; Ropers, C. Ultrafast low-energy electron diffraction in transmission resolves polymer/graphene superstructure dynamics. *Science* **2014**, *345*, 200−204.
(15) Müller, M.; Paarmann, A.; Ernstorfer, R. Femtosecond electrons probing currents and atomic structure in nanomaterials. *Nat. Commun.* **2014**, *5*, 5292.
(16) Lobastov, V. A.; Weissenrieder, J.; Tang, J.; Zewail, A. H. Ultrafast Electron Microscopy (UEM): Four-Dimensional Imaging and Diffraction of Nanostructures during Phase Transitions. *Nano Lett.* **2007**, *7*, 2552.
(17) Najafi, E.; Scarborough, T. D.; Tang, J.; Zewail, A. Four-dimensional imaging of carrier interface dynamics in p−n junctions. *Science* **2015**, *347*, 164−167.
(18) Beyer, A.; Gölzhäuser, A. Low energy electron point source microscopy: beyond imaging. *J. Phys.: Condens. Matter* **2010**, *22*, 343001.
(19) Sapoval, B.; Hermann, C. *Physics of Semiconductors*; Springer-Verlag: New York, 1995.
(20) Yu, L.; Zheng, J.; Xu, Y.; Dai, D.; He, S. Local and Nonlocal Optically Induced Transparency Effects in Graphene−Silicon Hybrid Nanophotonic Integrated Circuits. *ACS Nano* **2014**, *8*, 11386−11393.
(21) Merano, M.; Sonderegger, S.; Crottini, A.; Collin, S.; Renucci, P.; Pelucchi, E.; Malko, A.; Baier, M. H.; Kapon, E.; Deveaud, B.; Ganiere, J. D. Probing carrier dynamics in nanostructures by picosecond cathodoluminescence. *Nature* **2005**, *438*, 479−482.
(22) Gong, C.; Floresca, H. C.; Hinojos, D.; McDonnell, S.; Qin, X.; Hao, Y.; Jandhyala, S.; Mordi, G.; Kim, J.; Colombo, L.; Ruoff, R. S.; Kim, M. J.; Cho, K.; Wallace, R. M.; Chabal, Y. J. Rapid Selective Etching of PMMA Residues from Transferred Graphene by Carbon Dioxide. *J. Phys. Chem. C* **2013**, *117*, 23000−23008.
(23) Paarmann, A.; Gulde, M.; Muller, M.; Schafer, S.; Schweda, S.; Maiti, M.; Xu, C.; Hohage, T.; Schenk, F.; Ropers, C.; Ernstorfer, R. Coherent femtosecond low-energy single-electron pulses for time-resolved diffraction and imaging: A numerical study. *J. Appl. Phys.* **2012**, *112*, 112.
(24) Carbone, F.; Barwick, B.; Kwon, O.-H.; Park, H. S.; Baskin, J. S.; Zewail, A. H. EELS femtosecond resolved in 4D ultrafast electron microscopy. *Chem. Phys. Lett.* **2009**, *468*, 107−111.
(25) Carbone, F.; Kwon, O.-H.; Zewail, A. H. Dynamics of Chemical Bonding Mapped by Energy-Resolved 4D Electron Microscopy. *Science* **2009**, *325*, 181−184.
(26) Carbone, F. The interplay between structure and orbitals in the chemical bonding of graphite. *Chem. Phys. Lett.* **2010**, *496*, 291−295.
(27) Harb, M.; Jurgilaitis, A.; Enquist, H.; Nüske, R.; Schmising, C. v. K.; Gaudin, J.; Johnson, S. L.; Milne, C. J.; Beaud, P.; Vorobeva, E.; Caviezel, A.; Mariager, S. O.; Ingold, G.; Larsson, J. Picosecond dynamics of laser-induced strain in graphite. *Phys. Rev. B: Condens. Matter Mater. Phys.* **2011**, *84*, 045435.
(28) Carbone, F.; Baum, P.; Rudolf, P.; Zewail, A. H. Structural Preablation Dynamics of Graphite Observed by Ultrafast Electron Crystallography. *Phys. Rev. Lett.* **2008**, *100*, 035501.
(29) Raman, R. K.; Murooka, Y.; Ruan, C.-Y.; Yang, T.; Berber, S.; Tománek, D. Direct Observation of Optically Induced Transient Structures in Graphite Using Ultrafast Electron Crystallography. *Phys. Rev. Lett.* **2008**, *101*, 077401.
(30) Vakil, A.; Engheta, N. Transformation Optics Using Graphene. *Science* **2011**, *332*, 1291−1294.
(31) Park, S. T.; Yurtsever, A.; Baskin, J. S.; Zewail, A. H. Graphene-layered steps and their fields visualized by 4D electron microscopy. *Proc. Natl. Acad. Sci. U. S. A.* **2013**, *110*, 9277−9282.
(32) Thomas, S. J. M. The Renaissance and Promise of Electron Energy-Loss Spectroscopy. *Angew. Chem., Int. Ed.* **2009**, *48*, 8824−8826.
(33) Rust, M. J.; Bates, M.; Zhuang, X. Sub-diffraction-limit imaging by stochastic optical reconstruction microscopy (STORM). *Nat. Methods* **2006**, *3*, 793−796.
(34) Betzig, E.; Trautman, J. K.; Harris, T. D.; Weiner, J. S.; Kostelak, R. L. Breaking the Diffraction Barrier: Optical Microscopy on a Nanometric Scale. *Science* **1991**, *251*, 1468−1470.
(35) Zenhausern, F.; Martin, Y.; Wickramasinghe, H. K. Scanning Interferometric Apertureless Microscopy: Optical Imaging at 10 Angstrom Resolution. *Science* **1995**, *269*, 1083−1085.
(36) Tizei, L. H. G.; Kociak, M. Spectrally and spatially resolved cathodoluminescence of nanodiamonds: local variations of the NV^0 emission properties. *Nanotechnology* **2012**, *23*, 175702.
(37) Rossouw, D.; Botton, G. A. Plasmonic Response of Bent Silver Nanowires for Nanophotonic Subwavelength Waveguiding. *Phys. Rev. Lett.* **2013**, *110*, 066801.
(38) Barwick, B.; Flannigan, D.; Zewail, A. H. Photon Induced Near-Field Electron Microscopy. *Nature* **2009**, *462*, 902−906.
(39) Park, S. T.; Lin, M.; Zewail, A. H. Photon-induced near-field electron microscopy (PINEM): theoretical and experimental. *New J. Phys.* **2010**, *12*, 123028.
(40) Yurtsever, A.; van der Veen, R. M.; Zewail, A. H. Subparticle Ultrafast Spectrum Imaging in 4D Electron Microscopy. *Science* **2012**, *335*, 59−64.
(41) Yurtsever, A.; Zewail, A. H. Direct Visualization of Near-Fields in Nanoplasmonics and Nanophotonics. *Nano Lett.* **2012**, *12*, 3334−3338.
(42) Yurtsever, A.; Baskin, J. S.; Zewail, A. H. Entangled Nanoparticles: Discovery by Visualization in 4D Electron Microscopy. *Nano Lett.* **2012**, *12*, 5027−5032.
(43) Flannigan, D. J.; Barwick, B.; Zewail, A. H. Biological imaging with 4D ultrafast electron microscopy. *Proc. Natl. Acad. Sci. U. S. A.* **2010**, *107*, 9933−9937.
(44) Piazza, L.; Lummen, T. T. A.; Quinonez, E.; Murooka, Y.; Reed, B. W.; Barwick, B.; Carbone, F. Simultaneous observation of the quantization and the interference pattern of a plasmonic near field. *Nat. Commun.* **2015**, *6*, 6407.
(45) Feist, A.; Echternkamp, K. E.; Schauss, J.; Yalunin, S. V.; Schafer, S.; Ropers, C. Quantum coherent optical phase modulation in an ultrafast transmission electron microscope. *Nature* **2015**, *521*, 200−203.
(46) García de Abajo, F. J.; Asenjo-Garcia, A.; Kociak, M. Multiphoton Absorption and Emission by Interaction of Swift Electrons with Evanescent Light Fields. *Nano Lett.* **2010**, *10*, 1859−1863.
(47) Baum, P.; Zewail, A. H. Attosecond electron pulses for 4D diffraction and microscopy. *Proc. Natl. Acad. Sci. U. S. A.* **2007**, *104*, 18409−18414.

DOI: 10.1021/acsphotonics.5b00427
ACS Photonics 2015, 2, 1391−1402

(48) Hilbert, S. A.; Uiterwaal, C.; Barwick, B.; Batelaan, H.; Zewail, A. H. Temporal lenses for attosecond and femtosecond electron pulses. *Proc. Natl. Acad. Sci. U. S. A.* **2009**, *106*, 10558−10563.
(49) Fill, E.; Veisz, L.; Apolonski, A.; Krausz, F. Sub-fs electron pulses for ultrafast electron diffraction. *New J. Phys.* **2006**, *8*, 272.
(50) Mancini, G. F.; Mansart, B.; Pagano, S.; van der Geer, B.; de Loos, M.; Carbone, F. Design and implementation of a flexible beamline for fs electron diffraction experiments. *Nucl. Instrum. Methods Phys. Res., Sect. A* **2012**, *691*, 113−122.
(51) Kapteyn, H.; Cohen, O.; Christov, I.; Murnane, M. Harnessing attosecond science in the quest for coherent x-rays. *Science* **2007**, *317*, 775−778.
(52) Gibson, G.; Courtial, J.; Padgett, M.; Vasnetsov, M.; Pas'ko, V.; Barnett, S.; Franke-Arnold, S. Free-space information transfer using light beams carrying orbital angular momentum. *Opt. Express* **2004**, *12*, 5448−5456.
(53) McMorran, B. J.; Agrawal, A.; Anderson, I. M.; Herzing, A. A.; Lezec, H. J.; McClelland, J. J.; Unguris, J. Electron Vortex Beams with High Quanta of Orbital Angular Momentum. *Science* **2011**, *331*, 192−195.
(54) Asenjo-Garcia, A.; García de Abajo, F. J. Dichroism in the Interaction between Vortex Electron Beams, Plasmons, and Molecules. *Phys. Rev. Lett.* **2014**, *113*, 066102.
(55) Harvey, T. R.; Chess, J.; Pierce, J. S.; Ercius, P.; McMorran, B. J. Characterization of Electron Orbital Angular Momentum Transfer to Nanoparticle Plasmon Modes. *Microsc. Microanal.* **2014**, *20*, 68−69.
(56) Harvey, T. R.; Pierce, J. S.; Chess, J.; McMorran, B. J. Demonstration of electron helical dichroism as a local probe of chirality. *arXiv:1507.01810*, **2015**.
(57) Handali, J.; Shakya, P.; Barwick, B. Creating electron vortex beams with light. *Opt. Express* **2015**, *23*, 5236−5243.
(58) Glaeser, R. M.; Hall, R. J. Reaching the information limit in cryo-EM of biological macromolecules: Experimental aspects. *Biophys. J.* **2011**, *100*, 2331−2337.
(59) Majorovits, E.; Barton, B.; Schultheiß, K.; Pérez-Willard, F.; Gerthsen, D.; Schröder, R. R. Optimizing phase contrast in transmission electron microscopy with an electrostatic (Boersch) phase plate. *Ultramicroscopy* **2007**, *107*, 213−226.
(60) de Jonge, N.; Peckys, D. B.; Kremers, G. J.; Piston, D. W. Electron microscopy of whole cells in liquid with nanometer resolution. *Proc. Natl. Acad. Sci. U. S. A.* **2009**, *106*, 2159−2164.
(61) Glenn, D. R.; Zhang, H.; Kasthuri, N.; Schalek, R.; Lo, P. K.; Trifonov, A. S.; Park, H.; Lichtman, J. W.; Walsworth, R. L. Correlative light and electron microscopy using cathodoluminescence from nanoparticles with distinguishable colours. *Sci. Rep.* **2012**, *2*, 865.
(62) Densmore, A.; Vachon, M.; Xu, D. X.; Janz, S.; Ma, R.; Li, Y. H.; Lopinski, G.; Delâge, A.; Lapointe, J.; Luebbert, C. C.; Liu, Q. Y.; Cheben, P.; Schmid, J. H. Silicon photonic wire biosensor array for multiplexed real-time and label-free molecular detection. *Opt. Lett.* **2009**, *34*, 3598−3600.
(63) Lovell, J. F.; Jin, C. S.; Huynh, E.; Jin, H.; Kim, C.; Rubinstein, J. L.; Chan, W. C. W.; Cao, W.; Wang, L. V.; Zheng, G. Porphysome nanovesicles generated by porphyrin bilayers for use as multimodal biophotonic contrast agents. *Nat. Mater.* **2011**, *10*, 324−332.
(64) Homola, J. Present and future of surface plasmon resonance biosensors. *Anal. Bioanal. Chem.* **2003**, *377*, 528−539.
(65) Hsieh, H. V.; Pfeiffer, Z. A.; Amiss, T. J.; Sherman, D. B.; Pitner, J. B. Direct detection of glucose by surface plasmon resonance with bacterial glucose/galactose-binding protein. *Biosens. Bioelectron.* **2004**, *19*, 653−660.
(66) Yan, R.; Mestas, S. P.; Yuan, G.; Safaisini, R.; Dandy, D. S.; Lear, K. L. Label-free silicon photonic biosensor system with integrated detector array. *Lab Chip* **2009**, *9*, 2163−2168.
(67) Shen, H.; Lu, G.; Zhang, T.; Liu, J.; Gu, Y.; Perriat, P.; Martini, M.; Tillement, O.; Gong, Q. Shape effect on a single-nanoparticle-based plasmonic nanosensor. *Nanotechnology* **2013**, *24*, 285502.
(68) Herink, G.; Solli, D. R.; Gulde, M.; Ropers, C. Field-driven photoemission from nanostructures quenches the quiver motion. *Nature* **2012**, *483*, 190−193.
(69) Kruger, M.; Schenk, M.; Hommelhoff, P. Attosecond control of electrons emitted from a nanoscale metal tip. *Nature* **2011**, *475*, 78−81.
(70) Vogelsang, J.; Robin, J.; Nagy, B. J.; Dombi, P.; Rosenkranz, D.; Schiek, M.; Groß, P.; Lienau, C. Ultrafast Electron Emission from a Sharp Metal Nanotaper Driven by Adiabatic Nanofocusing of Surface Plasmons. *Nano Lett.* **2015**, *15*, 4685−4691.
(71) Baskin, J. S.; Liu, H.; Zewail, A. H. 4D multiple-cathode ultrafast electron microscopy. *Proc. Natl. Acad. Sci. U. S. A.* **2014**, *111*, 10479−10484.
(72) Eberlein, T.; Bangert, U.; Nair, R. R.; Jones, R.; Gass, M.; Bleloch, A. L.; Novoselov, K. S.; Geim, A.; Briddon, P. R. Plasmon spectroscopy of free-standing graphene films. *Phys. Rev. B: Condens. Matter Mater. Phys.* **2008**, *77*, 233406.
(73) Marinopoulos, A. G.; Reining, L.; Rubio, A.; Olevano, V. Ab initio study of the optical absorption and wave-vector-dependent dielectric response of graphite. *Phys. Rev. B: Condens. Matter Mater. Phys.* **2004**, *69*, 245419.
(74) Park, S. T.; Yurtsever, A.; Baskin, J. S.; Zewail, A. H. Graphene-layered steps and their fields visualized by 4D electron microscopy. *Proc. Natl. Acad. Sci. U. S. A.* **2013**, *110*, 9277−9282.
(75) Hassan, M. T.; Liu, H.; Baskin, J. S.; Zewail, A. H. Photon Gating in 4D Ultrafast Electron Microscopy. *Proc. Natl. Acad. Sci. U. S. A.* **2015**, to be published.

DOI: 10.1021/acsphotonics.5b00427
ACS Photonics 2015, 2, 1391−1402